Modeling interannual dense shelf water export in the region of the Mertz Glacier Tongue (1992-2007)

E. A. Cougnon, B. K. Galton-Fenzi, A. J. S. Meijers, B. Legresy

JOURNAL OF GEOPHYSICAL RESEARCH: OCEANS, VOL. 118, 5858–5872, doi:10.1002/2013JC008790, 2013

Modeling interannual dense shelf water export in the region of the Mertz Glacier Tongue (1992–2007)

E. A. Cougnon,[1,2,3] B. K. Galton-Fenzi,[3,4] A. J. S. Meijers,[5] and B. Legrésy[3,6]

Received 28 January 2013; revised 23 August 2013; accepted 30 September 2013; published 28 October 2013.

[1] Ocean observations around the Australian-Antarctic basin show the importance of coastal latent heat polynyas near the Mertz Glacier Tongue (MGT) to the formation of Dense Shelf Water (DSW) and associated Antarctic Bottom Water (AABW). Here, we use a regional ocean/ice shelf model to investigate the interannual variability of the export of DSW from the Adélie (west of the MGT) and the Mertz (east of the MGT) depressions from 1992 to 2007. The variability in the model is driven by changes in observed surface heat and salt fluxes. The model simulates an annual mean export of DSW through the Adélie sill of about 0.07 ± 0.06 Sv. From 1992 to 1998, the export of DSW through the Adélie (Mertz) sills peaked at 0.14 Sv (0.29 Sv) during July to November. During periods of mean to strong polynya activity (defined by the surface ocean heat loss), DSW formed in the Adélie depression can spread into the Mertz depression via the cavity under the MGT. An additional simulation, where ocean/ice shelf thermodynamics have been disabled, highlights the fact that models without ocean/ice shelf interaction processes will significantly overestimate rates of DSW export. The melt rates of the MGT are 1.2 ± 0.4 m yr^{-1} during periods of average to strong polynya activity and can increase to 3.8 ± 1.5 m/yr during periods of sustained weak polynya activity, due to the increased presence of relatively warmer water interacting with the base of the ice shelf. The increased melting of the MGT during a weak polynya state can cause further freshening of the DSW and ultimately limits the production of AABW.

Citation: Cougnon, E. A., B. K. Galton-Fenzi, A. J. S. Meijers, and B. Legrésy (2013), Modeling interannual dense shelf water export in the region of the Mertz Glacier Tongue (1992–2007), *J. Geophys. Res. Oceans*, *118*, 5858–5872, doi:10.1002/2013JC008790.

1. Introduction

[2] Antarctic Bottom Water (AABW) is an important part of the global thermohaline circulation and is known to form in the Weddell Sea, Ross Sea, and Adélie Land [*Rintoul*, 1998; *Orsi et al*., 1999; *Jacobs*, 2004]. More recently, AABW has been observed to form in the vicinity of Cape Darnley, located immediately west of the Amery Ice Shelf [*Tamura et al*., 2008; *Kusahara et al*., 2010; *Fukamachi et al*., 2010; *Ohshima et al*., 2013]. The Australian-Antarctic Basin (80°–150°E) contains two types of AABW, defined by their sources: Ross Sea Bottom Water enters the basin from the east and mixes with Adélie Land Bottom Water that is formed locally in geographically restricted latent heat polynyas around the East Antarctic coastline [*Rintoul*, 1998]. AABW in the Australian-Antarctic Basin has been observed to be freshening, possibly due to an increased supply of glacial meltwater from Antarctica [*Aoki et al*., 2005; *Rintoul*, 2007].

[3] The high rate of sea ice formation in latent heat polynyas and the associated brine rejection drive convection due to the formation of relatively dense water (e.g., High Salinity Shelf Water—HSSW). HSSW can sink below adjacent ice-shelves and drive basal melting of these ice-shelves leading to the creation of fresher Ice Shelf Water (ISW), which is defined as having a temperature below the surface freezing temperature [*Lewis and Perkin*, 1986]. The mixture of HSSW, ISW, and to some degree the overlying Circumpolar Deep Water (CDW) and Modified Circumpolar Deep Water (MCDW) can form Dense Shelf Water (DSW). DSW may be exported from the continental shelf, sinking into the deep ocean and mixing further with the MCDW, forming AABW. Changes in the volume of ISW and HSSW formed on the shelf can significantly alter subsequent formation rates of AABW at the continental shelf break [*Hellmer*, 2004; *Kusahara and Hasumi*, 2013].

[4] During the period of this study (1992–2007), the Mertz Glacier Polynya (MGP), centered at about 67°S and

[1]CSIRO-UTAS Quantitative Marine Sciences PhD Program, Institute for Marine and Antarctic Studies, University of Tasmania, Hobart, Tasmania, Australia.
[2]Commonwealth Scientific and Industrial Research Organisation, Marine and Atmospheric Research, Hobart, Australia.
[3]Antarctic Climate & Ecosystems Cooperative Research Centre, University of Tasmania, Hobart, Tasmania, Australia.
[4]Australian Antarctic Division, Kingston, Tasmania, Australia.
[5]British Antarctic Survey, Cambridge, UK.
[6]Laboratoire d'Etudes en Géophysique et Océanographie Spatiales (CNES-CNRS-UPS-IRD), UMR5566, Toulouse, France.

Corresponding author: E. A. Cougnon, CSIRO-UTAS Quantitative Marine Sciences PhD Program, Institute for Marine and Antarctic Studies, University of Tasmania, Private Bag 129, Hobart, Tas 7001, Australia. (eva.cougnon@utas.edu.au)

2169-9275/13/10.1002/2013JC008790

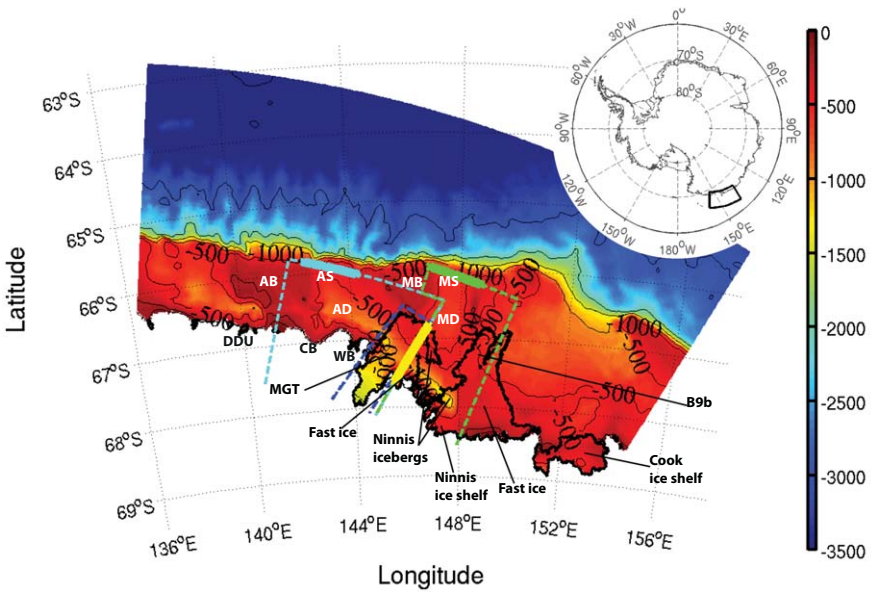

Figure 1. Bathymetry of the model and features of note around the Adélie and Mertz depressions. In the ocean: (AB: Adélie Bank; AD: Adélie Depression; AS: Adélie Sill; MB: Mertz Bank; MD: Mertz Depression; and MS: Mertz Sill), with the ice draft (dark line) of the Mertz Glacier Tongue (MGT; 140 km long, 25 km width), the B9b (with a draft of ∼300 m) and of the fast ice (∼ 30 m thick for the fast ice south east of the MGT and ∼ 10 m for the fast ice south east of B9b). Along the continent: Watts Bay (WB), Commonwealth Bay (CB), and Dumont D'Urville base (DDU). Cyan, green, and blue dashed lines indicate the boxes (Adélie, Mertz, and MGT boxes), used for averaging model results. The eastern edge of the cyan box is partially obscured by the green box and the yellow line. Cyan and green bold lines show the Adélie and Mertz sill section, respectively, and the yellow bold line along the MGT shows the cavity section.

145°E, was the second largest polynya in area (23,300 km^2) along the East Antarctic coastline [*Massom et al*., 2001] and was a key source of DSW that ultimately becomes AABW [*Rintoul*, 1998; *Williams and Bindoff*, 2003; *Williams et al*., 2008]. From satellite remote sensing observations, the MGP is estimated to produce an annual cumulative volume of sea ice of about 120 ± 11 km^3 yr^{-1} [*Tamura et al*., 2008]. The factors that influence the ice production of the MGP are the steep ice-sheet topography inland from Commonwealth Bay and Buchanan Bay (Figure 1) that funnel strong and persistent katabatic winds into the area, the distribution of grounded icebergs and surrounding fast ice, and the position of the Mertz Glacier floating ice Tongue (MGT) and other icebergs (like the large grounded iceberg B9b) which form a barrier against westward moving sea ice [*Massom et al*., 2001]. The MGT was 20–40 km wide and extended 150 km northward from the grounded ice-sheet, prior to its calving in 2010, which cut its length in half.

[5] Direct observations of the ocean in the vicinity of the MGT during winter are rare, due to the extreme conditions making access difficult. The first and the only wintertime experiment in the Adélie region occurred in July to August 1999 [*Bindoff et al*., 2001; *Williams and Bindoff*, 2003; *Williams et al*., 2008]. This wintertime experiment and associated summer observations have shown that DSW accumulates in the Adélie depression, and the Adélie sill is one of the primary outflow regions for dense water to escape from the depression to the abyssal ocean [*Bindoff et al*., 2000; *Williams et al*., 2008]. The annual mean export of DSW through the Adélie sill was estimated to be 0.1–0.5 Sv [*Williams et al*., 2008], subsequently revised down to 0.073 ± 0.083 Sv using improved analysis methods (Meijers et al., manuscripts in preparation). DSW exported at the sill depth (425 m) is dense enough relative to the offshore water masses to mix down the continental slope and slope canyons to form AABW [*Williams et al*., 2008]. More recent observations taken along the slope and over the deep ocean suggest that the Mertz sill, to the east of the MGT, may also be a region of DSW export [*Williams et al*., 2010]. The region to the east of the MGT also has a deep depression, called the Mertz depression or Trough, a sill (600 m) and an active local polynya in the lee of B9b. Modeling results also support the hypothesis that the Mertz sill is a key region of DSW export from the Mertz depression to the continental slope [*Kusahara et al*., 2011].

[6] Earlier model studies such as *Marsland et al*. [2004] using the Mertz-HOPE (Hamburg Ocean Primitive Equation) model (as described by *Marsland et al*. [2007]) and *Kusahara et al*. [2011] using the Center for Climate System Research Ocean Component (COCO) model [*Hasumi*, 2006], have studied the Adélie/Mertz depressions area. Both are coupled sea-ice/ocean models and have a global domain with high horizontal resolution over the study area. Neither of these studies include ice shelf/ocean interaction processes the circulation underneath ice-shelves or the formation of ISW. Our study uses a high resolution (∼2.16–2.88 km) regional ocean model, based on the Regional

Ocean Modeling System (ROMS) [*Shchepetkin and McWilliams*, 2005] to study the interannual variability of DSW export from the Adélie and Mertz depressions region from 1992 to 2007. The model is unique in that it has been modified to include ice shelf/ocean interactions and frazil dynamics and thermodynamics, and includes the ocean cavity beneath the MGT and other ice-shelves, icebergs, and fast ice in the region [following *Galton-Fenzi*, 2009, 2010; *Galton-Fenzi et al*., 2012]. *Marsland et al*. [2004] have shown a strong interannual variability of DSW outflow from the Adélie depression linked to variability in atmospheric forcing. In this study, we investigate the link between the variability of the surface polynya forcing and the shelf water, and how it impacts the density and volume of exported DSW.

[7] Section 2 describes the model setup and forcing, and details the analysis procedure. A similar approach to *Marsland et al*. [2004], using heat flux variability, is used in section 3 to define different polynya states. Using these polynya states, we examine relationships between the intensity of polynyas and dense water export, and the interactions with the ice shelf. In sections 4 and 5, we discuss key findings relating to dense water export. These include the different pathways for DSW export and the importance of including the cavity under the MGT, as well as the link between polynya activity and DSW export in comparison with previous model studies.

2. Methods

2.1. Model and Forcing

[8] The three-dimensional ice shelf/ocean cavity model used here is based on the Rutgers version of the Regional Ocean Modeling System (ROMS) [*Shchepetkin and McWilliams*, 2005]. ROMS has a free surface and uses a terrain-following vertical s-coordinate system controlled by the applied surface pressure, which has been adapted to allow the coordinates to follow the ice-shelf draft [*Dinniman et al*., 2003] and has been applied to other area of Antarctica [*Dinniman et al*., 2007; *Mueller et al*., 2012]. The version of the model we use here was initially developed for studies of the Amery Ice Shelf/Ocean system [*Galton-Fenzi*, 2009; *Galton-Fenzi et al*., 2012] and used in circum-Antarctic modeling studies [*Galton-Fenzi*, 2010]. In the region of our study, a version of this model has been used to simulate the circulation patterns and water mass properties in the vicinity of the Adélie and Mertz depressions [*Hemery et al*., 2011; *Cottin et al*., 2012]. It has also been compared directly with summertime ship observations and year long current meter moorings at the Adélie sill and found to accurately reproduce the seasonality and circulation within the depression (Meijers et al., manuscripts in preparation).

[9] The model setup used here is similar to the one described by *Galton-Fenzi et al*. [2012] and only the major features and differences from the previous model are described below. The model includes realistic tides and thermodynamic interactions with the ice shelf, including the addition of a frazil subroutine. The ice shelf/ocean interaction is described by three equations representing the conservation of heat, salt, and a linearized version of the freezing point of seawater (as a function of salinity and pressure) [e.g., *Holland and Jenkins*, 1999], which are solved to simultaneously find the temperature and salinity in the boundary layer beneath the ice shelf and the melt rate at the ice shelf base. The model grid extends from 135.77°E (west of the French base Dumont D'Urville) to east of George V land at 158.08°E and covers the Adélie and Mertz depressions from the coast line up to the deep ocean at 62.72°S (Figure 1). The horizontal grid has a resolution of about 2.16 km near the southern boundary and 2.88 km near the northern boundary. The vertical grid uses 31 contour following σ levels, arranged to give higher resolution near the top and the bottom of the water column.

[10] The bathymetry and ice-shelf draft is based on RTopo-1 [*Timmermann et al*., 2010] and was modified to include local high-resolution bathymetry data from *Beaman et al*. [2011], which is based on multibeam swath sonar and singlebeam bathymetry data with about 250 m resolution. The iceberg positions present in the region, and the MGT ice draft were created using high-resolution SPOT5 imagery, radar profiles from *Legrésy et al*. [2004], and a more recent airborne radio echo sounding (ICECAP project from International Polar Year and *Greenbaum et al*. [2010]). The bathymetry beneath the MGT has been created to accommodate the grounding line position and its thickness [*Legrésy et al*., 2004; *Mayet et al.*, 2013]. The ice draft of the MGT is shown in Figure 5, while the B9b icebergs have a draft of 300 m and Ninnis icebergs have a comparable thickness. Fast ice is an important factor to consider in the region because of its thickness and its multiannual presence in some areas [*Massom et al*., 2009]. We include a climatology from *Fraser et al*. [2012], which produces two main areas of permanent fast ice near the MGT. These regions are southeast of the ice tongue and southeast of the B9b iceberg, where fast ice is continuously present with a relatively constant area (see Figure 1). Southeast of the MGT fast ice attached to the glacier tongue is relatively old (at least 25 years) and thick (from 10 to 55 m). This is about 10 times thicker than the mean thickness of pack ice in the region [*Massom et al*., 2010].

[11] Following *Galton-Fenzi et al*. [2012], the model is forced with monthly data over the period from January 1992 to December 2007. Previous studies highlighted the importance of small-scale features, such as grounded icebergs, many of which are only a few hundred meters in scale. These features are important for the formation of polynyas and lead to localized enhanced DSW production [*Kusahara et al*., 2010]. However, coastal polynya and icebergs are often poorly resolved or are not parameterized in models, and so no sea ice model is coupled to the ocean in the present study. Instead, heat and salt fluxes, based on ice concentration from a climatology derived model using Special Sensor Microwave Imager (SSM/I) observations from 1992 to 2007 [*Tamura et al*., 2008, 2011], are used to adequately resolve the fine-scale polynya in the region, as has been done for other similar studies as *Dinniman et al*. [2003, 2007]. During summer, the *Tamura et al*. [2008] data are supplemented with open-water heat and salt fluxes using monthly climatologies from NCEP-2 [*Kanamitsu et al*., 2002]. Surface winds are derived from the second version of CORE data developed by *Large and Yeager* [2009] for global ocean-ice

modeling [*Griffies et al*., 2009]. The surface kinematic wind stress, τ, is calculated in the i direction and j direction from the wind velocity field, u as:

$$\tau_{i,j} = \rho_a c_a \mathbf{u}_{i,j} |\mathbf{u}_{i,j}|$$

where ρ_a is the air density (1.3 kg m^{-3}) and c_a is the dimensionless air-sea friction coefficient (1.4×10^{-3}). Lateral boundary fields, including potential temperature, salinity, and horizontal velocities are relaxed to monthly fields from ECCO2 over the period [*Menemenlis et al*., 2008; *Wunsch et al*., 2009]. The model was run for 48 years, including a spinup phase of 32 years to reach equilibrium using a repeating loop of synoptic forcing from 1992 to 2007. The final 16 years are used in the analysis.

2.2. Analysis Regions and Experiments

[12] To investigate the exchange between both shelf depressions and the export of DSW over the shelf break, our analysis is focused on three boxes around the Adélie and Mertz depressions and the MGT (Figure 1), and on three sections at the Mertz and Adélie sills and at the MGT cavity. These regions are chosen so as to facilitate comparisons with other studies [*Marsland et al*., 2004; *Kusahara et al*., 2011; Meijers et al., manuscripts in preparation]. The variables that are examined are potential temperature, salinity, horizontal velocities, and the volume transport of the main water mass classes (defined below). The boxes chosen completely surround the MGT in order to investigate the circulation through the cavity and ISW formation. They also include both the Adélie and Mertz depressions and their corresponding polynya areas, where the formation of shelf water occurs, and finally include both sills, where the export of DSW from the depressions is thought to occur [*Williams et al*., 2010; *Kusahara et al*., 2011].

[13] Different types of water interact within our study area, coming from offshore or forming over the shelf (Table 1). Antarctic Surface Water (AASW) is relatively warm and is the least dense water mass in the region, appearing at the surface. Below the surface offshore there is warm and saline CDW, and the deepest water mass off the shelf break is AABW. CDW moves southward and becomes Modified CDW (MCDW) through mixing with AASW and water over the shelf, before crossing the shelf break and entering the shelf region in the mid-water column where it can interact with HSSW and ISW created during sea ice formation and ice tongue melting, respectively. Low Salinity Shelf Water (LSSW) corresponds to a water mass similar to the HSSW in potential temperature but with a salinity less than 34.5 psu. We define DSW here as any water having a potential density greater than 1027.88 kg m^{-3}. This potential density has been used in previous studies as being the minimum potential density capable of sinking off the shelf and reaching abyssal depths, eventually contributing to the formation of AABW [*Bindoff et al*., 2001; *Williams et al*., 2008; *Kusahara et al*., 2010].

[14] To highlight the importance of considering ocean/ice shelf thermodynamics in modeling studies of shelf processed and dense water export, two experiments are performed for this paper: (1) "Reference simulation": the reference simulation uses the best version of the model described above, including ice shelf/ocean thermodynamics. (2) "Without ice shelf thermodynamics": reference simulation, but without ice shelf basal melting/freezing, so no ISW will be generated.

Table 1. Water Masses Defined by Potential Temperature (θ), Salinity (S), and Potential Density (ρ)

Water Type	θ (°C)	S (psu)	ρ (kg m^{-3} −1000)
AASW	$-1.75 \le \theta \le 2$		$\rho \le 27.75$
MCDW	$-1.75 \le \theta < 1$		$27.75 < \rho < 27.88$
HSSW	$\text{fp}^a < \theta < -1.75$	$S > 34.5$	
LSSW	$\text{fp}^a < \theta < -1.75$	$S \le 34.5$	
ISW	$\theta \le \text{fp}^a$		
DSW			$\rho \ge 27.88$

[a]fp is the in situ freezing temperature of sea water at 50 dbar.

3. Results

3.1. Polynya Activity

[15] The 16 year time series of heat fluxes from *Tamura et al*. [2008, 2011] shows an interannual variability in polynya activity (intensity) in the region (Figure 2). This figure shows the cumulative heat flux anomalies and the average wintertime heat flux anomalies for a fixed size area including both the Adélie and Mertz depressions (black line). It also shows those anomalies for smaller areas, one centered on the Mertz Glacier Polynya (MGP) over the Adélie depression (dashed line) and the other on the polynya in the lee of B9b iceberg over the Mertz depression (dotted line). The polynya activity is slightly different between the MGP and the region over the B9b polynya, but not dramatically so. For simplicity, we define the state of polynya activity as changes over the combined area of the depressions. The cumulative heat flux anomalies from monthly means over the Adélie and Mertz depressions (Figure 2a), shows a sudden change in polynya activity occurring in 2002. A positive cumulative flux trend indicates that the flux of heat from the ocean to the atmosphere is less than the normal trend over the whole period, and therefore indicates a decrease in polynya activity. A negative trend in polynya activity indicates intensified heat loss and increased polynya strength. In Figure 2a, interannual variability is observed with a net increased cumulative flux from 1999 to 2001 inclusive (about +550 MJ m^{-2}) with a sudden change in 2002 and a strong decrease of the cumulative flux until 2004 (about −600 MJ m^{-2}). From 1992 to 1996, the cumulative heat flux anomalies are relatively constant before increasing from 1997 to 1999 (+300 MJ m^{-2}), although at a weaker rate than from 1999 to 2001.

[16] The average heat flux anomalies (Figure 2b) for the wintertime average (from May to September inclusive) show the same pattern in terms of interannual variability, with the same two key periods of polynya activity. The period from 1999 to 2001 inclusive has a wintertime positive heat flux anomaly of approximately 8 ± 4 W m^{-2}, corresponding to a "weak polynya state." The period from 2002 to 2004 inclusive has a wintertime negative heat flux anomaly of approximately -11 ± 3 W m^{-2}, corresponding to a "strong polynya state." It is more difficult to define persistent strong or weak states for the other years because

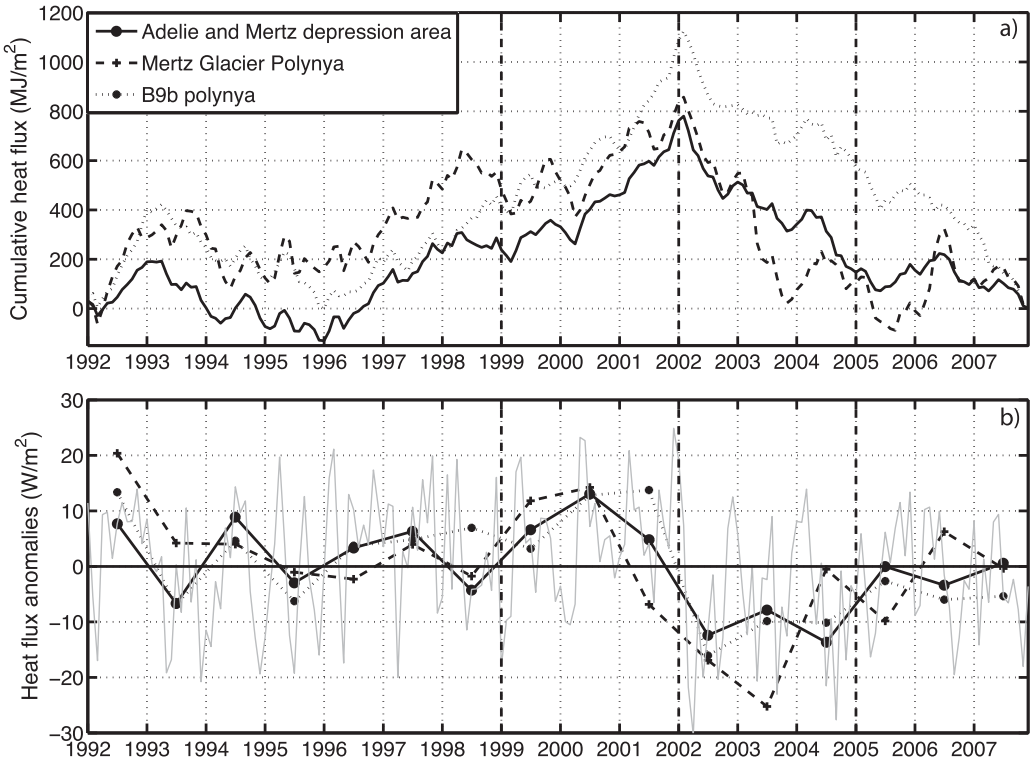

Figure 2. (a) Cumulative heat flux anomalies for the shelf fixed size area including both the Adélie and Mertz depressions (black line), for a small fixed size area over the Adélie depression (Mertz Glacier Polynya, dashed line), and a small fixed size area over the Mertz depression (B9b polynya, dotted line). Vertical dashed lines show the different states in polynya activity described in the text. (b) Heat flux anomalies for monthly means from *Tamura et al*. [2011] (fine gray line) and wintertime averages from May to September inclusive over the shelf area including both Adélie and Mertz depressions (black line with dots), the Adélie depression (Mertz Glacier Polynya, dashed line), and the Mertz depression (B9b polynya, dotted line). Negative anomalies indicate increased polynya strength and Dense Shelf Water formation.

negative heat flux anomalies alternate with positive anomalies each year, corresponding to a constant cumulative heat flux. We therefore call the period from 1992 to 1998 the "mean polynya state." *Marsland et al*. [2004] defined similar periods in polynya activity for the years in which the studies overlap (1992–2001). They defined a strong polynya state from 1993 to 1999, corresponding to the "mean" polynya state in our study, and weak polynya years (1999 and 2000) corresponding with our weak polynya state. As our study is longer, we define another period of "strong" polynya activity from 2002 to 2005.

3.2. Transport From the Adélie and Mertz Depressions

[17] The export by time for each density class between 1027.65 kg m^{-3} and 1028.00 kg m^{-3} is shown in the colored plots of Figure 3. The export is binned in density increments of 0.01 kg m^{-3} for the Adélie and Mertz boxes and both sills. This export is calculated as monthly averages over the entire period (from 1992 to 2007). The critical DSW density limit (1027.88 kg m^{-3}) is represented by the horizontal dashed line. Figure 3 clearly shows interannual variability in the export of DSW for both depressions and sills, but also seasonal variability. The minimum density for exported water is denser at the end of each winter and slightly lighter during summer, and does not always exceed the critical value. Over the 16 study years, three distinct periods of DSW export can be defined, as indicated by the vertical dashed lines. The first period is from 1992 to 1998, where the DSW export is strong for the Adélie box, and the two sills, associated with an import of the densest DSW into the Mertz box. 1999 is a transition year with lighter water exported, too light to be considered DSW but dense enough to be still exported from the Adélie box. This transition period is followed by a second period from 2000 to 2002, where there is almost no export of DSW from any of the boxes and sections. The last period is from 2003 to 2005 where there is an increase of DSW export mainly seen to flow out of the Adélie box and circulate through the cavity to the Mertz box. These periods lag the previously defined periods of polynya activity (shown by the arrows in the figure) by about a year.

[18] Different water masses can share the same density characteristics, so it is therefore useful to consider the transport results presented in Figure 3 together with potential temperature and salinity characteristics to determine the transport pathways of each of the main water masses. Figure 4 shows the net transport across both boxes and sills binned by potential temperature and salinity, averaged over the periods 1992–1998, 2000–2002, and 2003–2005. This projection allows us to see the different water masses that enter and exit each depression. The different water masses

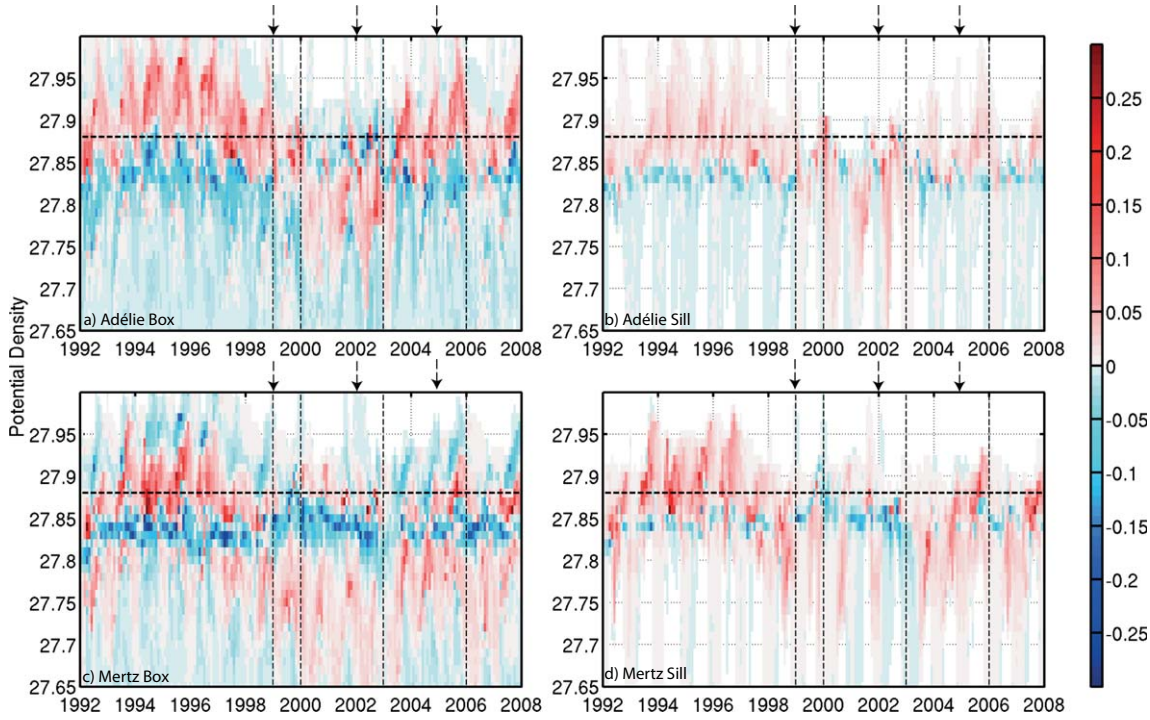

Figure 3. Transport (in Sv) by potential density class (in kg m^{-3} −1000) for each box and sill. Positives values (red) correspond to an export; negative values (blue) correspond to an import. Horizontal dashed line is the critical density 1027.88 kg m^{-3}. Vertical dashed lines show the limits of different states of DSW export, as discussed in the text. The arrows at the top of each plot show the transition between polynya activity states.

defined in Table 1 are labeled in Figure 4a, and we focus on the variability of the four main water masses: MCDW, HSSW, ISW, and DSW. ISW is defined here to be colder than the freezing temperature of sea water at 50 dbar. Using a depth below the surface is a necessary condition so that very shallow ISW produced by melting of thick fast ice east of the MGT (at about 35 m) is excluded. The averaged transport for each water mass (in 10^3 m^3 s^{-1} or milli-Sverdrups) and period for the Adélie and Mertz boxes and sills, and also for the cavity are summarized in Tables 2a–2c. Averages are also calculated for each case during the annual "peak export" period, which is defined as July to November, following *Marsland et al*. [2004] and which also corresponds to the peak dense water formation from observations [*Williams et al*., 2008].

[19] The density transport for both the Adélie and Mertz depressions differs between each period. However, in all three periods there is an import of relatively warm MCDW (between 0°C and 0.5°C, see Figures 4a–4c and 4g–4i) with a density between1027.80 kg m^{-3} and 1027.85 kg m^{-3}. For the Adélie box, an export of water denser than 1027.85 kg m^{-3} (dense enough to exist below the imported MCDW) is seen for both the first period (1992–1998) and the last period (2003–2005). This contributes to an export of DSW of 378 mSv for the first period and of 273 mSv for the last (Table 2a). During the first period, 29% of the DSW exported from the Adélie depression flows out through the Adélie sill (110 mSv), while only 19% goes through the sill during the last period (51 mSv). During the second period, the export is less dense, more spread in terms of density and salinity, and is only marginally denser than the imported water, so there is very little net DSW exported through the sill (<30 mSv).

[20] An export of very salty and dense HSSW is observed from the Adélie box with a transport of 212 mSv and 159 mSv for each period, respectively. This export has the same characteristics as the very dense water imported into the Mertz box (Figures 4g–4i). The circulation through the cavity section makes up a large proportion of the total DSW transport: 43% of the exported DSW formed in the Adélie depression is going through the cavity (165 mSv) during the first period and 46% (127 mSv) during the last period. This implies that 28% of DSW formed in the Adélie depression during the first period and 35% during the last period exits the box through pathways other than beneath the cavity or through the sill. These other pathways are discussed further in section 4.2.

[21] DSW that circulates beneath the MGT from the Adélie depression appears as an import into the Mertz box and is the sole pathway of DSW into the Mertz box through lateral boundaries. The 120 mSv exported out of the Mertz box are formed in the Mertz depression, primarily from the polynya in the lee of B9b, which is two third less than the DSW produced in the Adélie depression. The distribution of the water exported through the Mertz sill, in terms of density, shows a small import of MCDW (Figures 4j–4l), coupled with an export of cooler MCDW. Also, 207 mSv of DSW is exported through the sill during the first period significantly more than the net depression export. During the last period 69 mSv of DSW goes out through the Mertz sill, while the

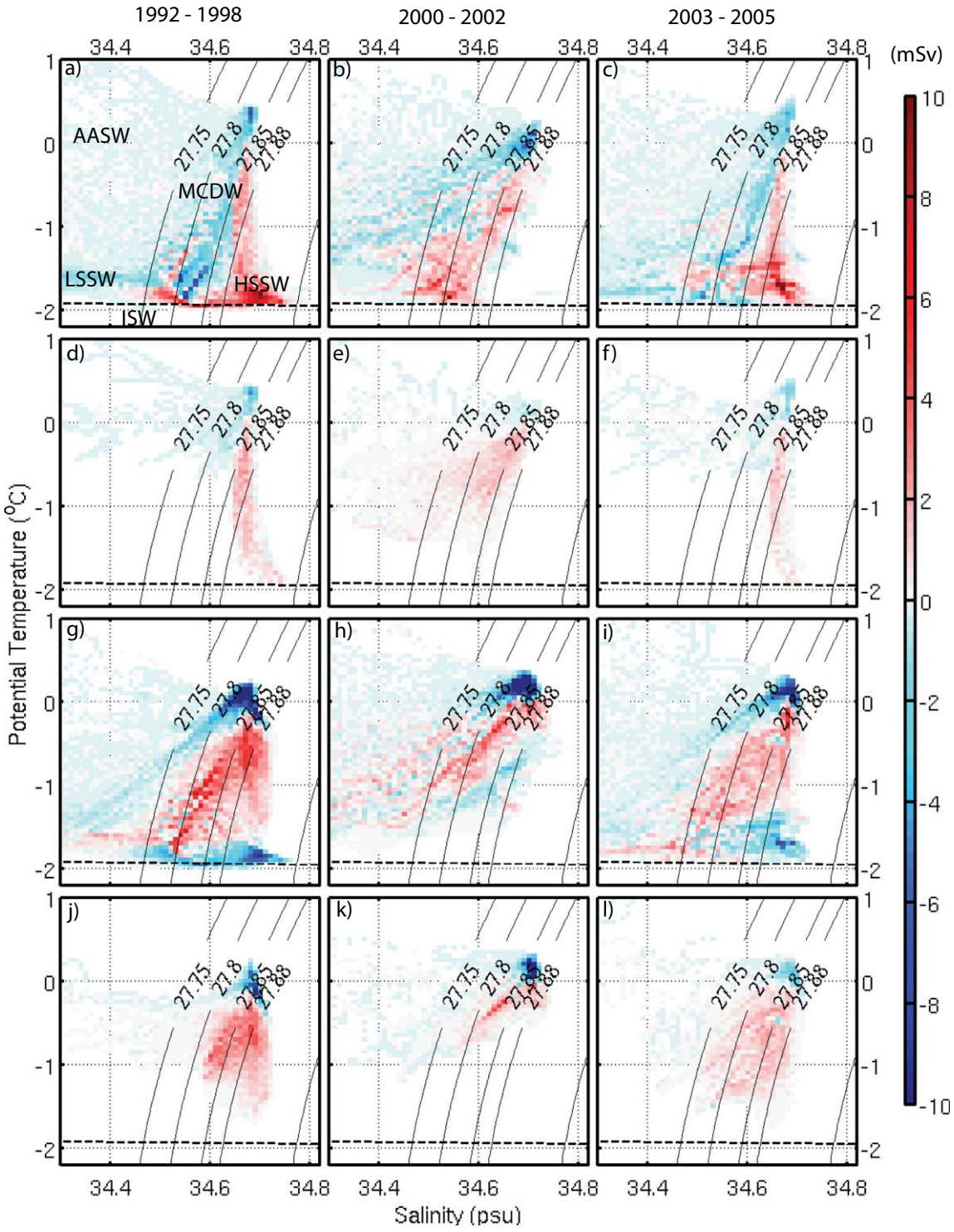

Figure 4. Potential temperature-salinity transport diagrams for the (a, b, c) Adélie box and (d, e, f) sill, and (g, h, i) Mertz box and (j, k, l) sill, split by period. Positive values (red) correspond to an export, and negative values (blue) correspond to an import (in milli Sv). Water masses are shown on the top left plot. Some potential density contours are shown on each diagram, with a dashed line corresponding to the freezing temperature of sea water at 50 dbar, used to define ISW in this study.

global DSW transport over the entire Mertz box shows an import of 35 mSv. This highlights the importance of the Adélie depression as the primary source of DSW and of the circulation beneath the MGT. During the second period, associated with weak polynya forcing, there is only a weak export of DSW (<50 mSv) from the whole Mertz box.

Table 2. Net Export for Each Period From (a) the Adélie Box and Sill and (b) for the Mertz Box and Sill for the Different Water Masses (milli Sv) From Table 1[a]

	Mean (1992–1998)		Weak (2000–2002)		Strong (2003–2005)	
	Entire Period	Peak Period	Entire Period	Peak Period	Entire Period	Peak Period
(a)						
Adélie Box						
AASW	−97	−91	−197	−199	−75	−55
MCDW	−310	−394	94	63	−154	−296
HSSW	212	281	108	140	159	220
LSSW	−12	−15	37	40	−43	−58
ISW	61	91	9	12	31	47
DSW	378	490	−15	−15	273	440
Adélie Sill						
MCDW	2	−4	188	76	7	−46
HSSW	16	23	10	14	11	18
ISW	5	9	1	0	4	7
DSW	110	138	30	20	51	74
(b)						
Mertz Box						
AASW	−66	−62	139	99	−60	−84
MCDW	−23	−24	−253	−143	84	131
HSSW	−127	−182	7	0	−70	−94
LSSW	−16	−29	−10	−31	8	2
ISW	−40	−55	1	0	−11	−19
DSW	120	116	48	16	−35	−62
Mertz Sill						
MCDW	162	194	−60	55	225	312
HSSW	11	13	0	0	17	28
ISW	1	1	0	0	2	3
DSW	207	286	23	44	69	114
(c)						
Cavity						
MCDW	−26	−42	41	150	45	39
HSSW	151	224	−5	3	119	181
ISW	40	56	−1	0	18	29
DSW	165	260	22	58	127	214

[a]Positive values correspond to an export and negative values to an import. The peak period corresponds to an average over each period from July to November.

3.3. Transport and Melting in the Mertz Glacier Tongue Cavity

[22] In this section, we examine the transport through the cavity. DSW formed in the Adélie depression flows into the MGT cavity on its western side, interacting with the ice shelf and mixing with ISW, leading to an export of slightly fresher and lighter water into the Mertz depression from the eastern side of the MGT. The difference between the second (weak) and the first (mean) periods in θ and S along the section defined by the MGT box are shown in Figures 5a and 5b. The third period (strong) is similar to the first, so anomalies from this period are not shown. The second period is mostly fresher and warmer everywhere along the section, except at about 400 m along the northern part of the MGT where a warm and salty anomaly occurs (of about $+1^{\circ}$C and $+0.04$ psu). The perpendicular velocity across the MGT transects over both periods (Figures 5c and 5d) shows a corresponding change in the circulation and magnitude along the northern part of the MGT at about 400 m. Import into the cavity at depth increases on the western boundary of the MGT, and a current can also be seen crossing the northeasterly tip of the MGT, heading in a southeasterly direction between 400 and 600 m. This is indicative of an import of MCDW under the northern part of the MGT during the period of weak polynya activity.

[23] The change in circulation impacts MGT melting (Figure 6). The area-averaged melt rate, integrated over the whole MGT for the entire period, is 1.9 ± 1.4 m yr^{-1} (11.4 ± 8.4 Gt yr^{-1}). For ice deeper than 900 m, melt rates are 4.5 ± 2.3 m yr^{-1} (3.0 ± 1.5 Gt yr^{-1}, not shown). The standard deviations of these values indicate the large temporal variability due to tidal, seasonal, and interannual forcing on the tongue. Observational estimates of melt rates, from flux gate calculations close to the grounding line vary from 11 m yr^{-1} [*Berthier et al*., 2003] to 18 m yr^{-1} [*Rignot*, 2002]. Given that 14–18 Gt yr^{-1} of ice is estimated to flow into the MGT from the grounded ice sheet [*Wendler et al*., 1996; *Frezzotti et al*., 1998], our estimates of basal melting indicate that about 63–81% of the total ice flowing into the MGT is melting from the underside, underlining how important it is to understand the ice-ocean interactions.

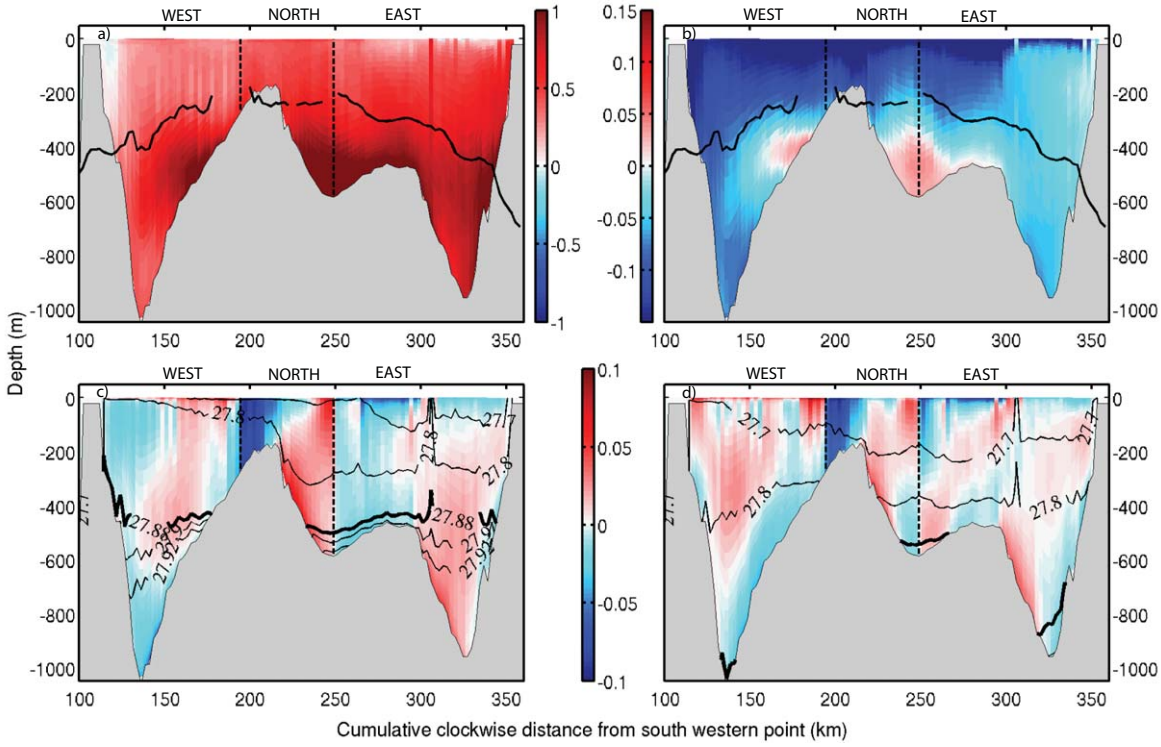

Figure 5. Differences in potential (a) temperature and (b) salinity for the MGT box between the second (2000–2002) minus the first (1992–1998) periods. The black line on Figures 5a and 5b shows the MGT ice draft for each edge of the ice tongue. (c and d) show the perpendicular velocity through the MGT box sections for the first and second period respectively (m s^{-1}), with potential density contours. Positive values are out of the MGT box.

[24] Figure 6 shows that the period of greatest net melt (3.8 ± 1.5 m yr^{-1}) occurs during the second (weak) period of polynya activity (2000–2002 inclusive) with the maximum melt rate (<8.5 m yr^{-1}) occurring during the summer of 2002/2003. Melting starts to decrease in 2003, corresponding to the beginning of the third (strong) period, when the export of dense water increases again. The area-averaged melt rate for the first and the third periods is 1.2 ± 0.4 m yr^{-1}. Despite the enhanced melting only small amounts of ISW, defined here as having a potential temperature below the freezing temperature at 50 dbar, are exported from beneath the MGT during the second period. This suggests that the additional glacial meltwater is warmer than our defined freezing temperature, and so is not classified as ISW and therefore likely to have been produced by warm MCDW during melting.

3.4. Sensitivity of Dense Shelf Water Export to Glacial Meltwater

[25] A recent study by *Kusahara and Hasumi* [2013] has shown the importance of including basal melting in modeling studies such as that one. To test the effect of having ice shelf thermodynamics in our model, a comparison between both the reference simulation and the simulation without ocean/ice shelf thermodynamics are presented in this section. Ocean/ice shelf thermodynamics in the model allows the formation of fresh and supercooled water due to ice shelf melting, which can mix with the surrounding dense water. *Hellmer* [2004] has shown that a decrease in ice shelf area with an associated reduction of basal melting significantly changes shelf water characteristics and enhances the formation of DSW.

[26] Figure 7 shows monthly climatologies of both simulations along both sills and along the cavity section on the eastern edge of the MGT. The simulation without ocean/ice shelf thermodynamics shows denser water in the cavity (~0.06 kg m^{-3} denser) and at both sills (~0.02 kg m^{-3} denser). Associated with this increased in density, a greater transport of DSW through these sections is also seen. Around 0.05 Sv more DSW flows from the Adélie to Mertz depression, but over 0.30 Sv extra is exported from the Mertz sill. Table 3 summarizes the averaged transport through the studied sections.

[27] The simulation without ocean/ice shelf thermodynamic overestimates DSW export by different magnitudes depending on the region. Compared to the reference simulation, DSW export is 100% greater for the Adélie sill and 50% larger for the entire Adélie box. However, for the Mertz box, omitting ocean/ice shelf thermodynamics induces an overestimation of DSW export of more than 500%. This very large increase in DSW export through the whole Mertz box is explained by the presence of more ice shelves in the Mertz box area (MGT, B9b, Ninnis icebergs, and fast ice). This relatively larger ice area in the Mertz depression induces greater volume of fresh and supercooled water, which mixes with the dense water imported from the Adélie depression and produced locally, and results in lighter and cooler DSW.

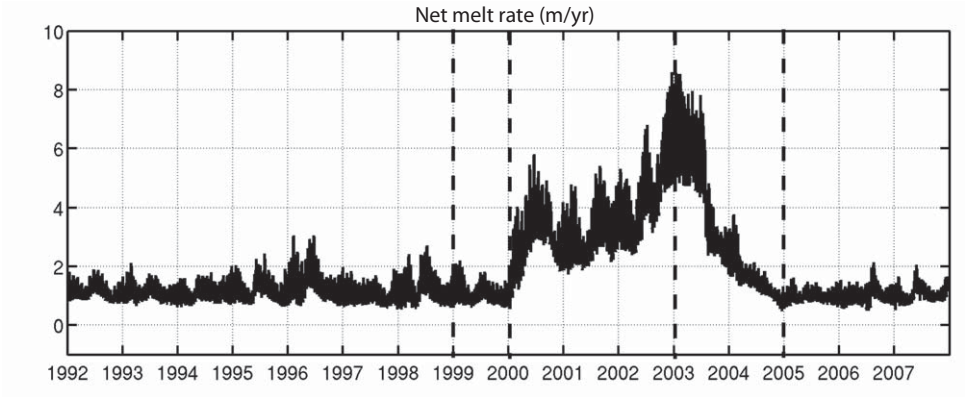

Figure 6. Net melt rate from the Mertz Glacier Tongue (in m yr^{-1}), combining the mass lost from the ice tongue and the accumulation of frazil ice. Vertical dashed lines show the same polynya transitions as in Figure 3.

4. Discussion

4.1. Links Between Polynya Activity, Ice Shelf Melting, and DSW Export

[28] Our results show a delay between the timing of the strength of polynya activity and the corresponding change in dense water export, not seen in previous studies. The weaker export, from 2000 to 2002, is delayed by about a year after the weakest polynya activity occurs during 1999 to 2001. The strongest polynya state (2002–2004) induces an increased DSW export in volume and density steadily over all three years from 2003 to 2005. However, this export remains on average less dense than during the first period (1992–1998). This difference in density export between the two periods suggests that after a period of weak polynya activity leading to a decrease of DSW export, three or more years of strong polynya activity are needed to precondition the density of shelf water to support the export of very dense water again. It is interesting to note that during the "mean" polynya state, there is a stronger export of the densest DSW than during the "strong" polynya state. This is likely due to the spinup period of the model. For the 32 spinup years prior to 1992, the model uses the same forcing (1992–2007), so the water masses at 1992 for the "mean" polynya state have been preconditioned by the last years of the atmospheric forcing, driving stronger net export.

[29] The interannual variability in the basal melt rate of the MGT follows the same pattern as the DSW export. Whilst the MGT is melting at a rapid rate between 2000 and 2002 (3.8 ± 1.5 m yr^{-1}), only small amounts of ISW are seen passing through the analysis boxes used in this study. During this time, the glacial meltwater that is produced must mix with the warmer ambient water and form a watermass that contains glacial meltwater which is warmer than our definition of ISW.

[30] During the weak polynya state, MCDW penetrates further on-shelf, although the actual volume entering the Adélie box does not change significantly from the strong or mean states (2.3 Sv for 1992–1998, 2.1 Sv for 2000–2002, and 2.0 Sv for 2003–2005). The mechanism driving MCDW onto the shelf may be due to a combination of factors. In some regions, the primary mechanism causing MCDW to move on-shelf is changes in winds [e.g., *Steig et al*., 2012; *Dinniman et al*., 2012]. Alternatively, *St-Laurent et al*. [2012] demonstrates that a warm slope front current may be also guided on-shelf via troughs in the slope bathymetry.

[31] A detailed dynamical examination of the factors driving MCDW circulation onto the shelf is beyond the scope of the present study, although qualitatively the Mertz Bank does appear to be important in guiding intrusions toward the MGT (Figure 8). What we find, however, is that MCDW import is not correlated with changes in DSW export nor with changes in surface wind stress (not shown). This supports the findings of *Marsland et al*. [2004] who found that polynya buoyancy flux was the primary factor controlling DSW export and winds had little correlation with the DSW production. Of course, polynya activity is not independent from the winds, ocean temperature, or circulation and there exist complex feedbacks between these factors. However, polynya activity, as measured by heat flux, is representative of an integration of these atmospheric and oceanic terms for the purpose of this study, and we find that there exists a useful correlation with the strength of these polynyas driving DSW export.

[32] The lack of correlation between polynya activity and MCDW import does not imply that inflow from off the shelf is unimportant to the circulation. During weak polynya states, the intruding MCDW is not cooled as dramatically and may interact with the MGT and modify the ice shelf/ocean driven circulation [*Klinck and Dinniman*, 2010] by intensifying the ice pump mechanism through cavity enhanced basal melting [*Lewis and Perkin*, 1986]. MCDW driven basal melting makes the water fresher and more buoyant which causes it to rise along the bottom of the ice shelf. This buoyancy driven flow has the effect of pulling deeper water to the base of the ice shelf. This induces more ice shelf melting which may further decrease the formation and density of DSW in the region. This positive feedback between intruding warm MCDW and increased freshening is discussed further in the following section.

4.2. Regional Circulation

[33] The model allows the detailed examination of DSW export pathways from the region, and we find several more than have been previously assumed in observational studies. The time-averaged potential temperature and density at

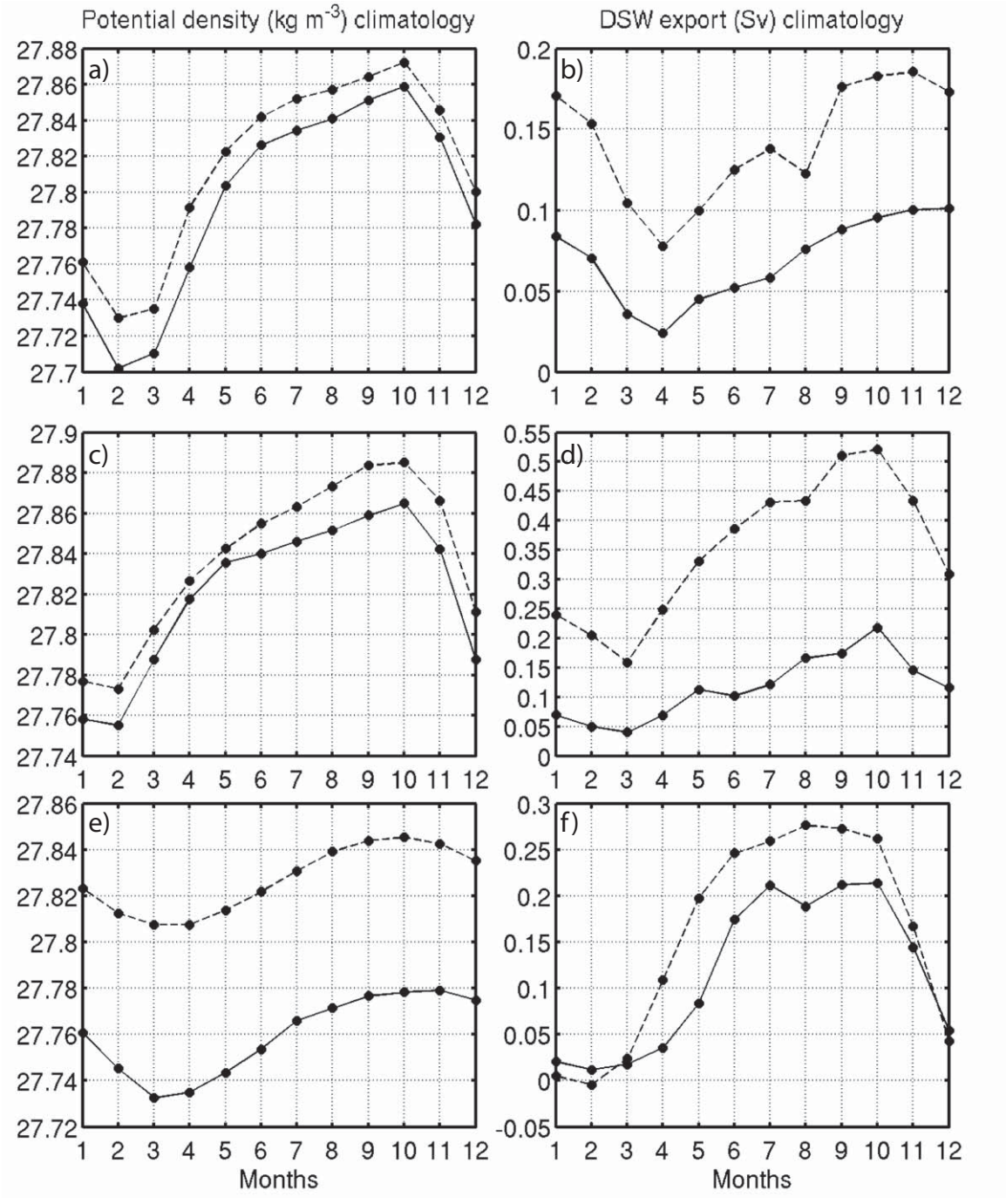

Figure 7. Monthly climatologies averaged over the entire period (1992–2007) for the potential density (left plots) and DSW transport (right plots) for the reference simulation (black line) and the simulation without ocean/ice shelf thermodynamics (dashed line) for (a and b) the Adélie sill, (c and d) the Mertz sill, and(e and f) the cavity section.

the model bottom layer, overlaid with the current direction during each period is shown in Figure 8. This figure shows that dense water spreads between both depressions through the MGT cavity and over the shelf break. Significant volumes of DSW are being exported from the Adélie box via the cavity under the MGT (120 mSv averaged over the entire period) as well as along the coast to the west (from the western edge of the Adélie box, 18 mSv averaged over the entire period). The heat flux forcing [*Tamura et al*., 2011] includes many small but active polynyas along the coast to the west of the MGT, such as in Commonwealth Bay. The model produces HSSW from these regions during winter and transports some DSW westward as part of the coastal current. However, observations do not find any circulation of DSW along the coast, likely because of their summertime bias. In the model during summer there is no HSSW production and DSW present in deep troughs and depressions does not easily escape the shelf region, except

Table 3. Comparison of Dense Water Export for Observations and Modeling studies (Sv); for This Study We Show Model Estimate of DSW Export Over the Period From 1992 to 2007, for Both Reference and Without Ocean/Ice Shelf Thermodynamics Simulations

Region	Export (Sv)	
This Study (1992–2007)		
	Reference Simulation	Without Ice Shelf Thermodynamics
Adélie box	0.24 ± 0.18	0.36 ± 0.11
Mertz box	0.05 ± 0.13	0.32 ± 0.26
Adélie sill	0.07 ± 0.06	0.14 ± 0.07
Mertz sill	0.12 ± 0.12	0.35 ± 0.22
Cavity	0.12 ± 0.07	0.16 ± 0.08
Marsland et al. [2004] (1991–2000)		
Adélie depression	0.15	
Kusahara et al. [2011] (1979–2008)		
Adélie sill	0.21 ± 0.05	
Mertz sill	0.12 ± 0.07	
Observations (Meijers et al., in preparation, 2008)		
Adélie sill	0.073 ± 0.083	

at the Adélie sill, as in observations [*Williams et al*., 2008]. Future wintertime observations should observe these water masses predicted by the model to establish the importance of export westward via the coastal current and outflows of the western edge of the basin.

[34] The off-shelf export is simulated to occur through both Adélie and Mertz sills and is also identified through another region located to the east of the Mertz sill (see black circles in Figures 8a and 8b), which export about 32 mSv of DSW averaged over the entire period. A significant part of the export going through the sills is missing in our current sill section locations. About 51 mSv of DSW, averaged over the entire period, is going throughout the western corner of the Adélie box and about 34 mSv throughout the western corner of the Mertz box directly west of the Mertz sill. This highlights the limitations of observational studies that only capture narrow regions of transport.

[35] The net export of DSW from the Mertz depression is greater at the sill than over the entire depression (Table 2b) due to the import from the Adélie depression via the cavity beneath the MGT. However, the DSW exported through the Mertz sill (with potential temperature between -1.5 and -0.5°C and a salinity below 34.5 psu) has different properties than the incoming DSW flow from the Adélie depression (colder than -1.5°C and sometimes saltier than 34.5 psu). This suggests that mixing occurs in the Mertz depression between DSW coming from the Adélie depression, the DSW or HSSW formed locally due to the polynya in the lee of B9b iceberg, ISW and overlying MCDW to produce relatively less dense DSW.

[36] The flow of DSW from the Adélie to the Mertz depression is strongly controlled by the activity of the MGT polynya. Figure 8 and Table 2 show clearly that during the first period there is significant formation of DSW, occurring mainly in the Adélie depression. The DSW created in the Adélie depression flows both into the cavity beneath the MGT and across the Adélie sill toward the abyssal ocean. In contrast, the second (weak) period has warmer bottom water, particularly over the Mertz depression and the northern edge of the MGT, and the water is significantly fresher on the Adélie and Mertz banks. Not enough DSW of sufficient volume and density is formed in the Adélie depression to enable the circulation to escape the shelf at the Adélie sill. Some DSW continues to circulate through the cavity and into the Mertz depression and through the sill but at much reduced rate. DSW starts to form again during winter 2003, mainly in the Adélie depression, which then spreads over the shelf to again escape through the Adélie sill at lower rate than during the first period, indicating a phase lag between the initial formation and eventual export of DSW. More than a year of strong polynya state is needed to form a sufficient volume and density of DSW to recover from the weak forcing period and to flow into the deep ocean.

[37] During the second period a reduced volume of ISW escapes the region, when we may have expected to see more due to the increased melt rates during this period. The extra melting is produced by enhanced MCDW penetration into the cavity. The warmer water mixes with the meltwater, resulting in a watermass warmer than the definition of ISW. Our results suggest that the commonly used definition of ISW that we have adopted for this study is inadequate for quantifying the amount of glacially sourced meltwater exported from the shelf.

[38] The additional freshwater produced by the MCDW intrusion and glacial melting may provide one possible explanation for the lag between enhanced polynya strength and the recovery of DSW export following a period of weak polynya activity. *Marsland et al*. [2004] showed that the volume averaged salinity within the Adélie Depression prior to the onset of winter polynya activity was an important "preconditioner" for DSW production and more saline preexisting watermasses led to stronger exports of DSW and vice versa. The enhanced melting of the MGT during weak polynya states may lead to such preconditioning of the water column, from which DSW export subsequently takes several years to recover. These dynamics are beyond the present study, however, and further examination is required to establish the impact of the enhanced buoyancy during weak polynya years.

4.3. Comparison With Other Studies

[39] Two other modeling studies, *Marsland et al*. [2004] and *Kusahara et al*. [2011], have examined this area using global domain ocean/sea-ice models, but neither include important ocean/ice shelf/fast-ice interaction processes or the circulation underneath ice-shelves. *Marsland et al*. [2004] used the years 1991–2000 to show an interannual variability in the wintertime heat flux, with weak (1991, 1992, 1999–2000) and strong (1993–1998 inclusive) states in the polynya activity corresponding to different states of circulation and magnitudes of DSW export from the region. *Kusahara et al*. [2011] also examined DSW export from the same region. The model was shown to reproduce key water masses of the region and a seasonal variability in the export of DSW through the Adélie sill linked to the seasonal sea-ice production in coastal polynyas area, but did not include ISW formation.

[40] The export of 100–500 mSv of DSW through the Adélie Sill observed in 1998 using ADCP moorings [*Williams et al*., 2008] is substantially higher than the

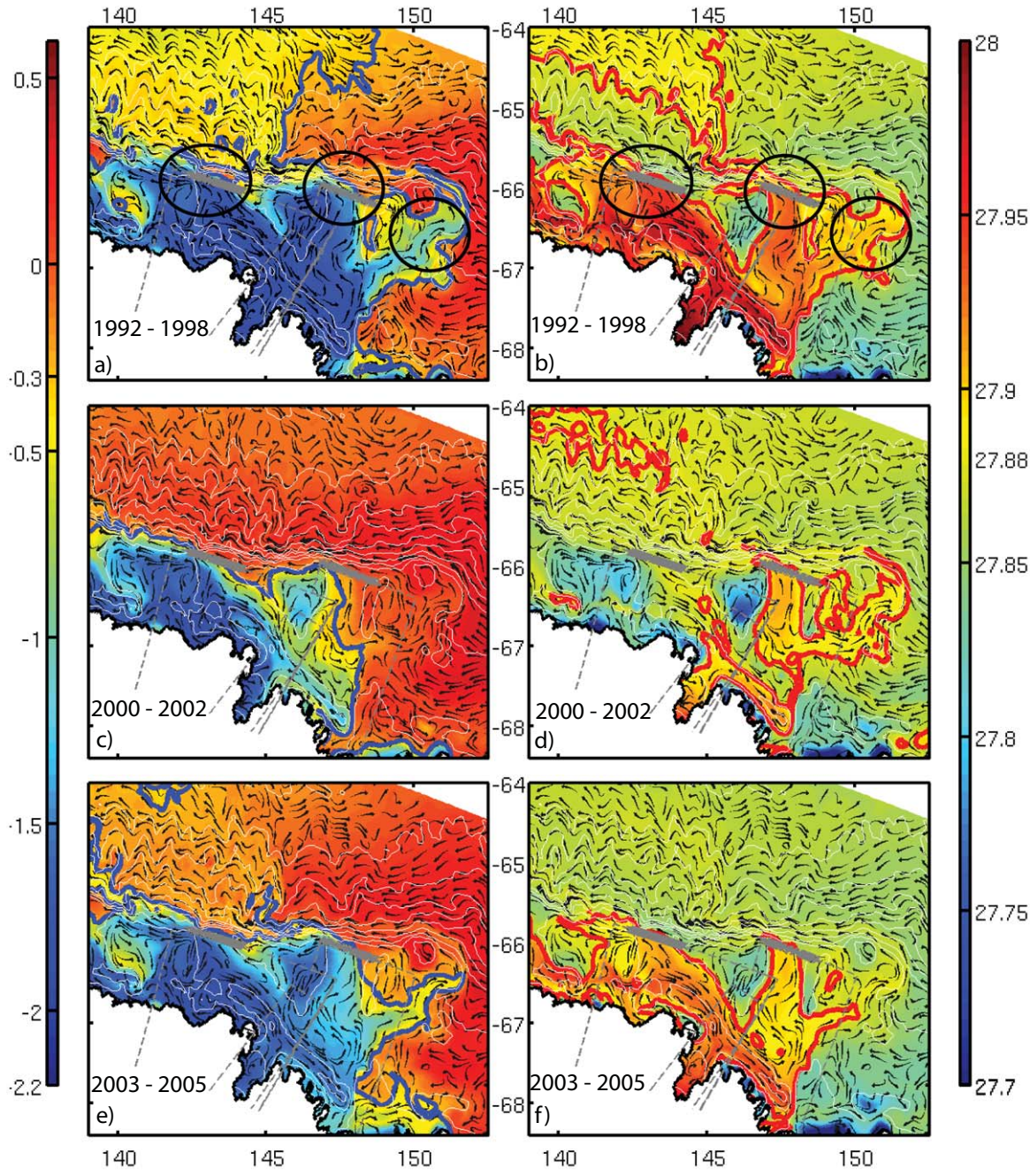

Figure 8. Potential temperature (left plots) and density (right plots), overlaid with velocity directions (arrows) averaged for each period at the bottom model layer. The velocity field is deduced from streamlines, but is indicative of direction only. The blue line on the potential temperature plots shows the −0.3°C isotherm, and the red line on the potential density plots is the critical limit for DSW export and AABW formation (1027.88 kg m^{-3}). Dashed lines show box boundaries, black circles show the three main areas of export, and white lines depth contours.

modeled value of 70 mSv with the current sill section. This difference may be explained, however, by the assumption made by *Williams et al*. [2008] that the measured current magnitude was directed entirely through the Adélie sill. This assumption was necessary due to the absence of compass heading measurements on the moorings, so the true current direction could not be determined. Subsequent observations using current meters with compasses measure substantially less transport directed through the sill (73 ± 83 mSv), which is in much closer agreement with the results from our study (Meijers et al., manuscripts in preparation).

[41] We show a net DSW export of 240 mSv from the Adélie depression compared to *Marsland et al*. [2004] who found 150 mSv. *Kusahara et al*. [2011] found a stronger export through the Adélie sill (210 mSv) than through the Mertz sill (120 mSv), which is the opposite of our pattern with 70 mSv for the Adélie sill and 120 mSv for the Mertz

sill. This difference in sill export is likely due to the circulation under the MGT connecting the two depressions, which is not included in either of the previous studies. Both earlier models consider the MGT as a land barrier separating the two depressions. As the polynyas are stronger in the Adélie depression area than in the Mertz depression area, *Kusahara et al*. [2011] therefore shows more DSW exported from the Adélie sill than from the Mertz sill. In our model, the connection between the basins via the MGT cavity enables both the melting of the MGT and the transport of DSW from the Adélie depression to influence the Mertz depression, and thus changes the ratio of DSW that is exported from each sill. In addition, both *Kusahara et al*. [2011] and *Marsland et al*. [2004] cannot produce ISW, which means they may overestimate both the amount and density of the DSW, as demonstrated here by the experiment where we shut off ocean/ice shelf thermodynamics, which showed that DSW export is up to 100% stronger.

5. Summary

[42] The region near the Mertz Glacier Tongue (MGT) is known to be a source of Dense Shelf Water (DSW) that contributes to the formation of Antarctic Bottom Water (AABW) [*Rintoul*, 1998; *Marsland et al*., 2004; *Williams et al*., 2008; *Kusahara et al*., 2011] and is associated with intense polynya activity. Here we have used a regional ice shelf/ocean model to investigate the shelf sea processes controlling the export of DSW from the continental shelf in the vicinity of the MGT. The model is improved over previous studies in that it includes ice shelf/ocean interaction processes, and a cavity beneath the MGT linking the two major regional shelf depressions. Modeled DSW export is in good agreement with available, although sparse, observations.

[43] Here we show that there is a delay of about a year between the change of polynya activity and the DSW export response. A single year of significantly weaker polynya activity can limit DSW export. A prolonged strong or mean polynya state (>1 year) is, however, needed for the volume of DSW on the continental shelf and depression to become large enough to escape the sill and move down slope to the abyssal ocean. We note, as previous studies have already done [*Williams et al*., 2010], that using a fixed critical density to define DSW is limiting and does not always capture the true export of DSW to the abyssal ocean. The critical value required for DSW to flow off-shelf should instead depend on the relative difference in the on-shelf DSW and the ambient off-shore water densities for greater accuracy.

[44] The connection between basins under the MGT allows dense water (mainly High Salinity Shelf Water—HSSW) from the Adélie depression to enter the Mertz depression as well as contributing to ice shelf basal melt. The glacial meltwater produced further decreases the density of DSW, and limits the net export of DSW. We highlight that models without ocean/ice shelf interaction processes will significantly overestimate rates of DSW and AABW export. We also show that in addition to the Adélie and Mertz sills DSW can also flow out of the continental shelf through the north eastern edge of the Mertz depression, and along the coast to the west of the Adélie depression, although whether or not these pathways contribute to AABW formation is unknown.

[45] Our study shows that DSW formed from active polynyas plays an important role in insulating ice shelves from melting by intrusions of relatively warm Modified Circumpolar Deep Water (MCDW). Here, our results suggest that during a sustained decrease in DSW formation, due to a reduction in the strength of the polynya activity (reduction in the strength of brine rejection), warm and salty MCDW will flow further on-shelf and drive higher ice shelf basal melting. The strong coupling between the polynya activity, DSW export and the basal melting of the MGT highlights the importance of understanding atmosphere-ocean-ice shelf interaction processes over the continental shelf seas, as well as exchange of water across the shelf break.

[46] We show that high interannual subglacial melting and the coupling between the polynya activity, the variability of the volume and the density of DSW and glacial meltwater is likely to be an important control on AABW variability. Unfortunately, the lack of long-term bottom water observations does not presently allow the evaluation of the interannual variability study in terms of DSW export and in terms of quantifying the AABW freshening due to atmospheric forcing.

[47] **Acknowledgments.** This work was supported by the Australian Government's Cooperative Research Centres Program through the Antarctic Climate & Ecosystems Cooperative Research Centre (ACE CRC) and by CNRS through the Laboratoire d'Etude en Géophysique et Océanographie Spatiale (LEGOS), France and the CRACICE project. Computing hours were provided by both the Tasmanian Partnership for Advanced Computing and the Australian National Computing Infrastructure under grant m68. The ROMS code was kindly provided by The ROMS/TOMS Group under the MIT/X License. We thank Simon Marsland (CSIRO, Australia) and Steve Rintoul (CSIRO, Australia), for helpful discussions during the development of the simulation. We also thank Lars Smedsrud (Geophysical Institute, University of Bergen), Scott Springer (Earth & Space Research, Seattle), and an anonymous reviewer for their constructive comments on the manuscript during the reviewing process.

References

Aoki, S., S. R. Rintoul, S. Ushio, and S. Watanabe (2005), Freshening of the Adélie land bottom water near 140oE, *Geophys. Res. Lett.*, *32*, L23601, doi:1029/2005GL024246.

Beaman, R. J., P. E. O'Brien, A. L. Post, and L. D. Santis (2011), A new high-resolution bathymetry model for the Terre Adélie and the George V continental margin, East Antarctica, *Antarct. Sci.*, *23*, 95–103, doi:10.1017/S095410201000074X.

Berthier, E., B. Raup, and T. Scambos (2003), New velocity map and mass-balance estimate of Mertz glacier, East Antarctica, derived from landsat sequential imagery, *J. Glaciol.*, *49*, 503–511.

Bindoff, N. L., S. R. Rintoul, and R. Massom (2000), Bottom water formation and polynyas in Adelie Land, Antarctica, *Pap. Proc. R. Soc. Tasmania*, *133*(3), 51–56.

Bindoff, N. L., G. D. Williams, and I. Allison (2001), Sea-ice growth and water mass modification in the Mertz Glacier polynya, East Antarctica, during winter, *Ann. Glaciol.*, *33*, 399–406.

Cottin, J., B. Raymond, A. Kato, F. Amélineau, Y. L. Maho, T. Raclot, B. Galton-Fenzi, A. Meijers, and Y. Ropert-Coudert (2012), Foraging strategies of male Adélie penguins during their first incubation trip in relation to environmental conditions, *Mar. Biol.*, *159*(8), 1843–1852, doi:10.1007/s00227-012-1974-x.

Dinniman, M., J. Klinck, and E. Hofmann (2012), Sensitivity of Circumpolar Deep Water transport and ice shelf basal melt along the west Antarctic Peninsula to changes in wind, *J. Clim.*, *25*(14), 4799–4816, doi:10.1175/JCLI-D-11–00307.1.

Dinniman, M. S., J. M. Klinck, and W. O. Smith Jr. (2003), Cross-shelf exchange in a model of the Ross Sea circulation and biogeochemistry, *Deep Sea Res., Part II*, *50*, 3103–3120.

Dinniman, M. S., J. M. Klinck, and W. O. Smith Jr. (2007), Influence of sea ice cover and icebergs on circulation and water mass formation in a numerical circulation model of the Ross Sea, Antarctica, *J. Geophys. Res.*, *112*, C11013, doi:10.1029/2006JC004036.

Fraser, A. D., R. A. Massom, K. J. Michael, B. K. Galton-Fenzi, and J. L. Lieser (2012), East Antarctic landfast sea ice distribution and variability, 2000–08, *J. Clim.*, *25*(4), 1137–1156.

Frezzotti, M., A. Cimbelli, and J. Ferrigno (1998), Ice-front change and iceberg behaviour along Oates and George V coasts, Antarctica, 1912–96, *Ann. Glaciol.*, *27*(167), 643–650.

Fukamachi, Y., K. I. Ohshima, S. Aoki, Y. Kitade, T. Tamura, and M. Wakatsuchi (2010), Antarctic Bottom Water revealed by mooring measurements off Cape Darnley, Antarctica, in *International Polar Year Oslo Science Conference*, Oslo, Norway, 8–12 Jun.

Galton-Fenzi, B. K. (2009), Modelling ice-shelf/ocean interaction, PhD thesis, Univ. of Tasmania, Hobart, Tasmania.

Galton-Fenzi, B. K. (2010), Modelling the interaction between Antarctica and the Southern Ocean, *Tech. Rep. 33*, edited by A. J. Hollis and K. A. Day, Cent. for Aust. Weather and Clim. Res. Tech. Rep.

Galton-Fenzi, B. K., J. R. Hunter, R. Coleman, S. J. Marsland, and R. Warner (2012), Numerical modelling of melt/freeze beneath the Amery Ice Shelf, *J. Geophys. Res.*, *117*, C09031, doi:10.1029/2012JC008214.

Greenbaum, J. S., D. D. Blankenship, D. A. Young, T. G. Richter, B. Legrésy, B. Galton-Fenzi, and Y. Gim (2010), Basal characteristics and inferred bathymetry beneath the Mertz Glacier Tongue, Antarctica, from coupled airborne radar sounding and gravity prior to the February 12th 2010 breakup event, in *4th SCAR Open Science Conference—Antarctica: Witness to the Past and Guide to the Future*, 3–6 Aug., Buenos Aires.

Griffies, S., et al. (2009), Coordinate Ocean-ice reference experiment (COREs), *Ocean Modell.*, *26*, 1–46.

Hasumi, H. (2006), Ocean Component Model (COCO) version 4.0, CCSR Rep. 25, Cent. for Clim. Syst. Res., Univ. of Tokyo.

Hellmer, H. H. (2004), Impact of Antarctic ice shelf basal melting on sea ice and deep ocean properties, *Geophys. Res. Lett.*, *31*, L10307, doi:10.1029/2004GL019506.

Hemery, L. G., B. K. Galton-Fenzi, N. Améziane, M. J. Riddle, S. R. Rintoul, R. J. Beaman, A. L. Post, and M. Eléaume (2011), Predicting habitat preferences for Anthometrina adriani (Echinodermata) on the East Antarctic continental shelf, *Mar. Ecol. Prog. Ser.*, *441*, 105–116, doi:10.3354/meps09330.

Holland, D. M., and A. Jenkins (1999), Modelling thermodynamic ice ocean interactions at the base of an ice shelf, *J. Phys. Oceanogr.*, *29*, 1787–1800.

Jacobs, S. S. (2004), Bottom water production and its link with the thermohaline circulation, *Antarct. Sci.*, *16*(4), 427–437.

Kanamitsu, M., W. Ebisuzaki, J. Woollen, S.-K. Yang, J. Hnilo, M. Fiorino, and G. Potter (2002), Ncep-doe amip-ii reanalysis (r-2), *Bull. Am. Meteorol. Soc.*, *83*(11), 1631–1643.

Klinck, J. M., and M. S. Dinniman (2010), Exchange across the shelf break at high southern latitudes, *Ocean Sci.*, *6*(2), 513–524, doi:10.5194/os-6-513-2010.

Kusahara, K., and H. Hasumi (2013), Modeling Antarctic ice shelf responses to future climate changes and impacts on the ocean, *J. Geophys. Res. Oceans*, *118*, 2454–2475, doi:10.1002/jgrc.20166.

Kusahara, K., H. Hasumi, and T. Tamura (2010), Modeling sea ice production and dense shelf water formation in coastal polynyas around East Antarctica, *J. Geophys. Res.*, *115*, C10006, doi:10.1029/2010JC006133.

Kusahara, K., H. Hasumi, and G. D. Williams (2011), Dense shelf water formation and brine-driven circulation in the Adélie and George V Land region, *Ocean Modell.*, *37*, 122–138.

Large, W. G., and S. G. Yeager (2009), The global climatology of an interannually air-sea flux data set, *Clim. Dyn.*, *33*, 341–364.

Legrésy, B., A. Wendt, I. Tabacco, F. Rémy, and R. Dietrich (2004), Influence of tides and tidal current on Mertz Glacier, Antarctica, *J. Glaciol.*, *50*(170), 427–435.

Lewis, E. L., and R. G. Perkin (1986), Ice pumps and their rates, *J. Geophys. Res.*, *91*(C10), 11,756–11,762.

Marsland, S. J., N. L. Bindoff, G. D. Williams, and W. F. Budd (2004), Modeling water mass formation in the Mertz Glacier Polynya and Adelie Depression, East Antarctica, *J. Geophys. Res. 109*, C11003, doi:10.1029/2004JC002441.

Marsland, S. J., H. Haak, J. H. Jungclaus, M. Latif, and F. Röske (2007), Antarctic coastal polynya response to climate change, *J. Geophys. Res.*, *112*, C07009, doi:10.1029/2005JC003291.

Massom, R. A., K. L. Hill, V. I. Lytle, A. P. Worby, M. J. Paget, and I. Allison (2001), Effects of regional fast-ice and iceberg distributions on the behaviour of the Mertz Glacier polynya, East Antarctica, *Ann. Glaciol.*, *33*, 391–398.

Massom, R. A., K. Hill, C. Barbraud, N. Adams, A. Ancel, L. Emmerson, and M. J. Pook (2009), Fast ice distribution in Aélie Land, East Antarctica: inter annual variability and implications for emperor penguins Aptenodytes forsteri, *Mar. Ecol. Prog. Ser.*, *374*, 243–257.

Massom, R. A., A. B. Giles, H. A. Fricker, R. C. Warner, B. Legrésy, G. Hyland, N. Young, and A. D. Fraser (2010), Examining the interaction between multi-year landfast sea ice and the Mertz Glacier Tongue, East Antarctica: Another factor in ice sheet stability?, *J. Geophys. Res.*, *115*, C12027, doi:10.1029/2009JC006083.

Mayet, C., L. Testut, B. Legresy, L. Lescarmontier, and F. Lyard (2013), High resolution barotropic modeling and the calving of the Mertz Glacier, East Antarctica, *J. Geophys. Res. Oceans*, 118, doi:10.1002/jgrc.20166.

Menemenlis, D., J. M. Campin, P. Heimbach, C. Hill, T. Lee, A. Nguyen, M. Schodlock, and H. Zhang (2008), ECCO2: High resolution global ocean and sea ice data synthesis, *Mercator Ocean Q. Newsl.*, *31*, 13–21.

Mueller, R. D., L. Padman, M. S. Dinniman, S. Y. Erofeeva, H. A. Fricker, and M. A. King (2012), Impact of tide-topography interactions on basal melting of Larsen C Ice Shelf, Antarctica, *J. Geophys. Res.*, *117*, C05005, doi:10.1029/2011JC007263.

Ohshima, K. I., et al. (2013), Antarctic Bottom Water production by intense sea-ice formation in the Cape Darnley polynya, *Nat. Geosci.*, *6*, 235–240.

Orsi, A. H., G. C. Johnston, and J. B. Bullister (1999), Circulation, mixing and production of Antarctic Bottom Water, *Prog. Oceanogr.*, *43*(1), 55–109.

Rignot, E. (2002), Mass balance of East Antarctic glaciers and ice shelves from satellite data, *Ann. Glaciol.*, *34*(1), 217–227.

Rintoul, S. (1998), On the origin and influence of Adélie Land Bottom Water, in *Ocean, Ice, and Atmosphere: Interaction at the Antarctic Continental Margin, Antarct. Res. Ser.*, vol. *75*, edited by S. Jacobs and R. Weiss, pp. 151–172, AGU, Washington, D. C.

Rintoul, S. (2007), Rapid freshening of Antarctic Bottom Water formed in the Indian and Pacific oceans, *Geophys. Res. Lett.*, *34*, L06606, doi:10.1029/2006GL028550.

Shchepetkin, A. F., and J. C. McWilliams (2005), The Regional Oceanic Modeling system (ROMS): A split-explicit, free-surface, topography-following-coordinate oceanic model, *Ocean Modell.*, *9*, 347–404, doi:10.1016/j.ocemod.2004.08.002.

St-Laurent, P., J. M. Klinck, and M. S. Dinniman (2012), On the role of coastal troughs in the circulation of warm circumpolar deep water on Antarctic shelves, *J. Phys. Oceanogr.*, *43*, 51–64.

Steig, E. J., Q. Ding, D. S. Battisti, and A. Jenkins (2012), Tropical forcing of Circumpolar Deep Water Inflow and outlet glacier thinning in the Amundsen Sea Embayment, West Antarctica, *J. Glaciol. 53*(60), 19–28, doi:10.3189/2012AoG60A110.

Tamura, T., K. I. Ohshima, and S. Nihashi (2008), Mapping of sea ice production for Antarctic coastal polynyas, *Geophys. Res. Lett.*, *35*, L07606, doi:10.1029/2007GL032903.

Tamura, T., K. I. Ohshima, S. Nihashi, and H. Hasumi (2011), Estimation of surface heat/salt fluxes associated with sea ice growth/melt in the Southern Ocean, *SOLA*, *7*(0), 17–20.

Timmermann, R. et al. (2010), A consistent dataset of Antarctic ice sheet topography, cavity geometry, and global bathymetry, *Earth Syst. Sci. Data*, *3*, 231–257.

Wendler, G., K. Ahlna, and C. S. Lingle (1996), On Mertz and Ninnis glaciers, East Antarctica, *J. Glaciol.*, *42*(142), 447–453.

Williams, G. D., and N. L. Bindoff (2003), Wintertime oceanography of the Adélie Depression, *Deep Sea Res., Part II*, *50*, 1373–1392.

Williams, G. D., N. L. Bindoff, S. J. Marsland, and S. R. Rintoul (2008), Formation and export of dense shelf water from the Adélie Depression, East Antarctica, *J. Geophys. Res.*, *113*, 4039, doi:10.1029/2007JC004346.

Williams, G. D., S. Aoki, S. S. Jacobs, S. R. Rintoul, T. Tamura, and N. L. Bindoff (2010), Antarctic Bottom Water from the Adélie and George V Land coast, East Antarctica (140–149°E), *J. Geophys. Res. 115*, C04027, doi:10.1029/2009JC005812.

Wunsch, C., P. Heimbach, R. Ponte, I. Fukumori, and the ECCO-GODAE Consortium Members (2009), The global general circulation of the ocean estimated by the ECCO Consortium, *Oceanography*, *22*(2), 88–103.